Solar Physics
DOI: 10.1007/•••••-•••-•••-••••-•

# Coronal Shock Waves, EUV Waves, and their Relation to CMEs. III. Propagation of a Probable Coronal Shock Wave Produced in the 17 January 2010 Event

**V.V. Grechnev**[1] · **An.N. Afanasyev**[1] · **A.M. Uralov**[1] · **I.M. Chertok**[2] · **M.V. Eselevich**[1] · **V.G. Eselevich**[1] · **G.V. Rudenko**[1] · **Y. Kubo**[3]



**Abstract** We consider particularities of propagation of a probable coronal shock wave produced in the 17 January 2010 backside event. The shock front was traced from low coronal disturbances visible in extreme ultraviolet (EUV), a shock-driven plasma flow visible in white light, and a metric type II burst. We analyze shock propagation by using both the weak shock approximation and a power-law fit corresponding formally to the approximation of a strong self-similar shock. Expansion of the leading edge of a coronal transient and changes in its shape corresponded to an expected trace of a freely propagating coronal shock wave presumably excited by an abrupt filament eruption. Non-regular variations of the near-surface fast-mode speed affected brightness and sharpness of the EUV wave front, but did not determine its kinematics, which was governed by the large-scale coronal magnetic configuration. No indications of opening magnetic fields far from the eruption region have been revealed, whereas the EUV wave was detectable. On the other hand, correspondence between all wave signatures, the drift rate of the type II burst, expected propagation of a shock wave, and the fast-mode speed distribution support its shock-wave nature.

**Keywords:** Coronal Mass Ejections, Low Coronal Signatures; Coronal Mass Ejections, Initiation and Propagation; Radio Bursts, Type II; Waves, Shock

[1]Institute of Solar-Terrestrial Physics SB RAS, Lermontov St. 126A, Irkutsk 664033, Russia email: grechnev@iszf.irk.ru
[2] Pushkov Institute of Terrestrial Magnetism, Ionosphere and Radio Wave Propagation (IZMIRAN), Troitsk, Moscow Region, 142190 Russia email: ichertok@izmiran.ru
[3] National Institute of Information and Communications Technology, Tokyo, Japan email: kubo@nict.go.jp

## 1. Introduction

Efforts of researchers to understand the nature of large-scale wave-like disturbances observed in extreme ultraviolet (EUV) in association with coronal mass ejections (CMEs) and flares, and called EUV waves or "EIT waves" (Thompson *et al.*, 1998, 1999) meet difficulties due to insufficient temporal coverage by existing telescopes and other observational limitations (see Grechnev *et al.*, 2011; henceforth Paper I). EUV waves are faint with respect to flare emissions. They mostly propagate, but sometimes stand. Their properties appear to be diverse and contradictory. Deficiency of observational material stimulated development of conflicting concepts, whose essence can be mainly reduced to effects of transformations of coronal magnetic fields (Delannée and Aulanier, 1999; Chen *et al.*, 2002; Chen, Fang, and Shibata, 2005; Attrill *et al.*, 2007) or MHD disturbances (Warmuth *et al.*, 2001; Khan and Aurass, 2002; Long *et al.*, 2008; Gopalswamy *et al.*, 2009) both caused by a CME eruption (see also Zhukov and Auchère, 2004; reviews of Wills-Davey and Attrill, 2009; Gallagher and Long, 2010).

The launch in 2006 of the twin-spacecraft Solar-Terrestrial Relations Observatory (STEREO; Kaiser *et al.*, 2008) carrying the Sun Earth Connection Coronal and Heliospheric Investigation instrument suites (SECCHI; Howard *et al.*, 2008) significantly extended opportunities to study EUV waves with the Extreme Ultraviolet Imagers (EUVI). They supply us with detailed observations of EUV waves, significantly reducing the temporal undersampling problem. However, this has not resulted in consensus about their nature. A number of studies came to a conclusion about the shock-wave nature of observed EUV waves (*e.g.*, Kienreich, Temmer, and Veronig, 2009; Patsourakos and Vourlidas, 2009; Patsourakos *et al.*, 2009). On the other hand, Zhukov, Rodriguez, and de Patoul (2009) presented an EUV wave incompatible with the fast-mode wave interpretation. Disappointing was the study of the 19 May 2007 EUV wave, which was considered as evidence both in favor of the shock-wave hypothesis (Long *et al.*, 2008; Veronig, Temmer, and Vršnak, 2008; Gopalswamy *et al.*, 2009) and against it (Attrill, 2010; Yang and Chen, 2010). Even with a possible involvement of different phenomena, the fact that the conclusions about the same observation were opposite suggests that some of them might be incorrect (our analysis of this controversy in Paper I supports the shock-wave interpretation). A recent multi-temperature analysis of an EUV wave observed in still more detail with Solar Dynamics Observatory (SDO) provides more questions than answers (Liu *et al.*, 2010).

Diversity of EUV waves implies their probable relation to different CME-associated phenomena (Zhukov and Auchère, 2004; Grechnev *et al.*, 2008; Cohen *et al.*, 2009), although implication of some confusions or incorrect conclusions is not excluded. Our companion Papers I – III are devoted to EUV waves presumably associated with coronal shock waves. A long-standing challenge for the shock-wave hypothesis was a problem raised by Klassen *et al.* (2000), who did not find any correlation between the speeds of EUV waves and drift rates of type II radio bursts. Paper I has shown how presumably shock-related EUV waves, type II bursts, and leading edges of the corresponding CMEs could be reconciled. We have proposed a simple quantitative description for all of these phenomena based on an approach of a self-similar shock wave. The length of such a wave is large

and comparable with the curvature radius of the wave front. Its deceleration is determined by the mass augmentation rate inside the volume limited by the shock front. The self-similar approach adequately describes propagation of strong shock waves. Moreover, its usage in analyses of large-scale coronal waves revealed a convenient way to fit their kinematics with direction-depending power-law (PL) functions[1]. Afanasyev and Uralov (2011, henceforth Paper II) have considered the opposite limit of a rather weak shock calculated analytically in terms of the WKB approach taking account of nonlinear effects (hereafter WS model).

A favorable opportunity for a detailed analysis of an EUV wave was granted by the Sun on 17 January 2010. The eruption and wave were well observed with EUVI imager, and a related white-light coronal transient was registered with COR-1 coronagraph, both on the STEREO-Behind spacecraft. EIT telescope (Delaboudinière *et al.*, 1995) and LASCO/C3 coronagraph (Brueckner *et al.*, 1995) on SOHO also observed this event despite its backside location. A weak type II burst was recorded in the HiRAS (NICT, Japan) and Learmonth (US Air Force RSTN) spectrographs. Veronig *et al.* (2010) analyzed this event and concluded that the coronal transient observed both in EUV and white light was a dome of a 'weakly shocked fast-mode MHD wave'. In their opinion, the upward dome expansion was driven all the time. We analyzed the same event independently and also inferred the shock-wave nature of this coronal transient. However, the scopes of our and Veronig *et al.* (2010) studies do not coincide and differ in some particular statements. Our analysis shows that the shock wave was most likely excited by the impulsive-piston mechanism and freely propagated afterwards, so that our considerations in Paper I entirely apply to this event. Unlike Veronig *et al.* (2010), we have found deceleration of both near-surface and off-limb traces of the wave. We also compare our measurements from EUV and coronagraph images with the drift rate of the type II burst and model results.

In this paper we *i*) address some of issues, which Veronig *et al.* (2010) did not consider, *e.g.*, propagation of the wave on-disk and off-limb and its kinematics at larger distances; *ii*) explain the difference between our results and the authors' ones; *iii*) compare the results, which the self-similar shock approximation and modeling of a weak shock provide being applied to this particular event.

## 2. Analysis of Observations

The vantage points of the two STEREO spacecraft were 69.6° behind the Earth and 64.3° ahead of it. The eruption site was visible from STEREO-B at S25 E59 (heliolatitude $B0 = 3.74°$). It was located for observers on the Earth $\approx 37°$ behind the eastern limb with a projected position onto the visible solar surface of about S32 E55 ($B0 = -4.75°$). The 'epicenters' visible from the Earth (and SOHO) and STEREO-B were rather close to each other. The radial extent and velocity of ejecta drawing away from the Sun were smaller by a factor of 1.13 for

[1]The 'shock-PL' abbreviation denotes henceforth considerations of shock waves traveling in the solar atmosphere in the approximation of a self-similar shock propagating in medium with a power-low density falloff, as done in Paper I.

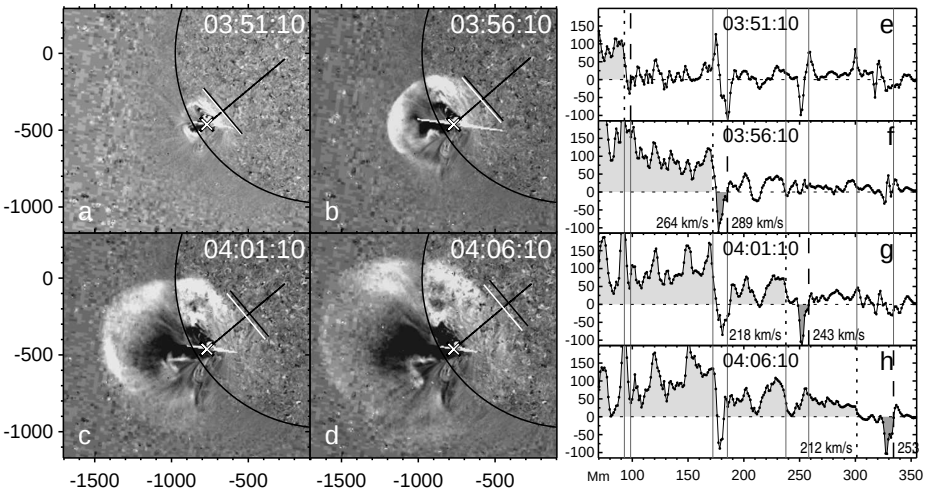


**Figure 1.** a – d) Four EUVI 195 Å images of the EUV wave and eruption. The slanted cross marks the eruption site. The black line going from the eruption site northwest shows the direction where the spatial profiles were computed. The white and black bars across it mark the presumable fronts suggested by the spatial profiles. In all EUVI images hereafter, the axes show arc seconds from the solar disk center as if viewed from the Earth. e – h) The spatial profiles of the EUV brightness measured in the direction shown in the left panels. The vertical broken lines extended with the solid gray lines denote presumable fronts. The shading indicates the EUV wave brightening behind the front and a possible negative precursor ahead.

observers on the Earth (SOHO) with respect to observations on STEREO-B. The COR-1 coronagraph on STEREO-A registered a wide transient around $\approx 225°$, but we do not consider either STEREO-A/COR-1 or SOHO/EIT observations.

### 2.1. Eruption and a Probable Shock Wave

Figure 1a – d shows the onset of the event observed in EUVI 195 Å fixed-base ratio images (see also the movie euvi_195.mpg accompanying the electronic version of our paper). A dome-like EUV wave expanded above the limb and propagated along the solar surface. The foremost boundary of the near-surface front passed into the off-limb dome suggesting their common nature. The front was followed by extended brightenings indicating a significant length of the disturbance. Eruption and subsequent untwisting of a magnetic rope structure is visible inside the EUV wave dome. The motion of the eruption was three-dimensional. Along with paling of the eruption and difficulties to distinguish it from the wave front, this makes measurements of its kinematics unreliable.

Figure 1e – h shows spatial profiles computed from the four fixed-base difference 195 Å images within narrow sectors of 1° along the directions indicated with black lines ($\approx 40°$ counter-clockwise from the western direction). The profiles show a complex surface relief. The chosen direction crosses compact features, which seem to have responded to the pass of the wave front. The EUV wave brightening appears in the profiles as an enhancement (highlighted with bright gray shading) to the left from the front (dotted). All the four profiles show compact darkening regions (dashed, darker shading) preceding the brightening.

The dashed and dotted lines in panels e – h correspond to the black and white bars in panels a – d. Comparison of all panels e – h with each other reveals slightly variable compact features at the four fixed positions, where the front presumably showed up. Hits by a shock front probably disturbed these features, producing the sharp effects suggested by the profiles, but not a gradual elevation. The EUVI pixel size (the samples are shown with small circles) was $\approx 1190$ km; with actual exposure times of 16 s, a step-like front moving with estimated plane-of-sky speeds shown in panels f – h must be caught in three to four pixels. Thus, just such a picture is expected when dealing with a shock front.

The quiet Sun's level in these images (computed as a highest-probability brightness inside the solar disk minus the sky level found in the same way) is about 290 counts/pixel. Comparison with the levels of the profiles shows that if the effect was real, then it was so strong (especially in the negative precursor) that could only be due to disturbance of low structures. Although the effect is marginal, it seems to deserve attention to be checked in other events.

Another result is more obvious. After the pass of the wave front, small features like coronal bright points got disturbed, but did not disappear (the euvi_195.mpg movie also shows this). This implies that closed magnetic fields in these configurations did not open. No signatures of magnetic reconnection are detectable.

The plane-of-sky velocities of the presumable fronts systematically decreased, despite propagation from the near-the-limb eruption site towards the solar disk center. The surface velocities of these fronts estimated using different ways all exceeded 390 km $s^{-1}$ initially and all were less than 290 km $s^{-1}$ finally.

### 2.2. Global EUV Wave Fronts

We were not satisfied with results of attempts to identify complete wave fronts and therefore divided the problem into two tasks: 1) identification of global fronts and 2) analysis of smaller-scale properties of EUV wave propagation. To reveal global wave fronts, we use ratios of running-difference images to preceding ones. The obtained images have been deeply filtered to reveal weak portions of the fronts. The result is shown in Figure 2 (eight of 12 images which we used). We separately outline the on-disk and off-limb parts of the fronts with red and pink ovals, trying to catch their outermost envelopes over a maximal spatial extent. To analyze kinematics, we measured the distances along the green great circle. The technique used by Veronig *et al.* (2010) was more sensitive. They analyzed spatial profiles computed within some sectors and searched for their foremost edges close to the visually identified fronts. The blue contours approximately reproduce the fronts, which the authors identified.

Figure 2 shows the following facts. 1) The fronts identified by Veronig *et al.* all lead our fronts with progressive increase of the distances between their fronts and our ones. 2) The southern portion of the wave front (indicated by the arrows in panels d and e) moved significantly faster in the environment of the polar coronal hole, while the fronts themselves were difficult to detect there. 3) The wave dome expanded non-radially: with the southeastern position of the eruption site, expansion of the dome was pointed almost exactly to the left in the plane of the sky. Also, the wave 'epicenter' (projection of the off-limb dome

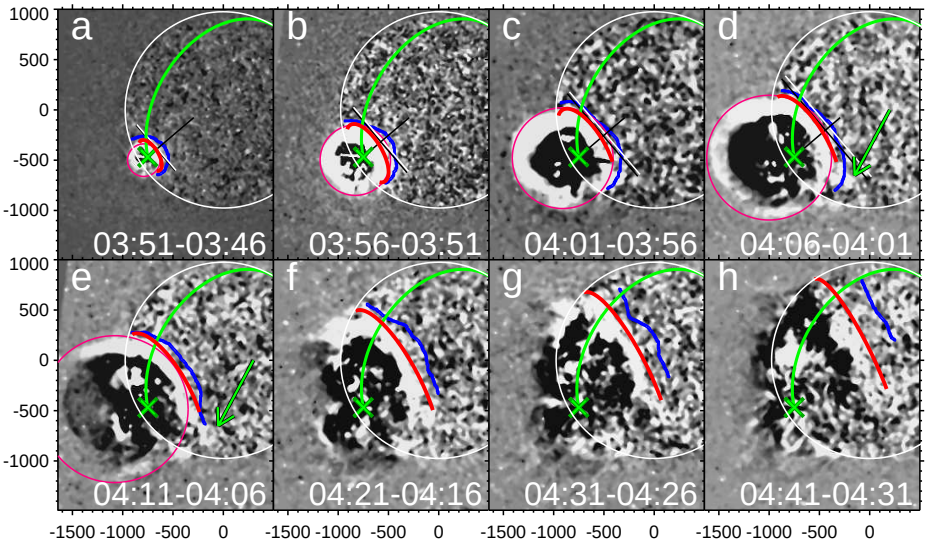


**Figure 2.** Global wave fronts in EUVI 195 Å images. The red arcs outline the leading edges of the global wave fronts detectable in the figure. The blue lines correspond to the fronts of Veronig *et al.* (2010). The pink ovals outline the off-limb wave dome. The arrows indicate a bend of the fronts around the South Pole coronal hole. Distances along the solar surface were measured from the eruption cite (the slanted cross) along the green great circle. The white and black bars mark the presumable fronts from Figure 1.

center onto the solar surface) increasingly shifted northeast, so that the fronts in later images were not parallel to the earlier ones (*cf., e.g.,* panels d and h).

The lag of the red fronts behind the blue ones is initially small and nearly constant, and then significantly increases. This implies deceleration of the red fronts, because measurements of Veronig *et al.* (2010) revealed a constant speed. Indeed, the distance-time plot of the red fronts presented later in Figures 7b and 8b (red symbols) shows deceleration, which is well fitted with a PL function expected for a shock wave (see Paper I). It is $x(t) = x_1[(t-t_0)/(t-t_1)]^{\alpha}$, where $t$ and $x$ are current time and distance, $t_0 = 03{:}47{:}48$ is the wave start time, $t_1$ and $x_1$ correspond to one of the measured fronts, and the PL exponent $\alpha = 2/(5-\delta)$ with $\delta$ being a density falloff index in this formal approximation. We fitted the kinematics of the wave front with an exponent of $\alpha \approx 0.82$ ($\delta \approx 2.53$) for surface propagation, and $\alpha \approx 0.91$ ($\delta \approx 2.8$) for off-limb expansion. The measurements of the velocities along the great circle have largest uncertainties at early stages of wave expansion. To specify the measurements in this initial interval, we used 171 Å images observed with a higher imaging rate.

Figure 3 presents four of 12 EUVI 171 Å images used in measurements. Since the shock-PL fit appears to match the situation, we applied here a different technique. Using parameters of the shock-PL fit found from 195 Å data as an initial approximation, we endeavored to outline each of the on-disk and off-limb wave portions with ovals calculated from the shock-PL fit according to the observation times. Parameters of the fit were specified in this way. If some parts of the wave fronts were not detectable, we used their other possible signatures.

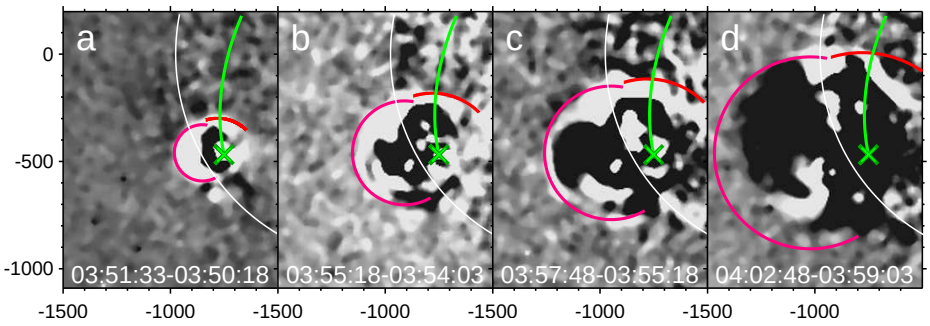


**Figure 3.** Global wave fronts detectable in EUVI 171 Å images and their outline. The red arcs outline the leading edges of the on-disk wave fronts detectable in the figure. The pink ovals outline the off-limb wave dome. The green arc denotes a great circle along which our measurements were made. The slanted green cross marks the eruption site.

An extreme example is shown in panel d. Here the reference regions for the off-limb oval were the upper (in the plane of the sky) brightening just above the limb and three faint lowermost compact regions. The on-disk oval was referred to the bright feature crossing the limb and a small portion of the wave front next to the former feature. The results of these measurements shown in Figure 7b and Figure 8b with blue triangles can also be fitted with a power law with $\delta = 2.74$ for the off-limb dome and $\delta = 2.1$ for surface propagation (blue curve).

### 2.3. EUV Wave Components and Fast-Mode Speed Distribution

The most effective way to reveal faint EUV waves is to use running difference images, which emphasize the outermost fronts, but the trailing picture in such images does not correspond to a real brightness distribution, and quasi-stationary manifestations disappear. The EUV wave in this event is well visible in fixed-base ratio images allowing one to see what happened behind the wave front. Seven such deeply filtered EUVI 195 Å ratio images are shown in Figure 4a – g. The whole large-scale brightening consisted of small patches. It was wide and was complex. The outer EUV wave front included another wide inner brightening, which adjoined the dimming. The off-limb part of the inner component (HF1) was visible for about half an hour up to 290 Mm.

A high feature HF2 (panel g) at about 230 Mm appeared when the wave front reached it. This feature was associated with a lower dense part of a coronal streamer that highlighted the wave front. Long loops connecting the active region with a southwestern area ('Loops' in panel d) also highlighted the wave. Most of these loops located aside of the active region did not show any stretch, although the wave front obviously passed through the loops. These properties are consistent with a wave nature of the outer EUV wave. The images do not reveal any manifestations of magnetic field opening aside of the eruption region, where the outer EUV wave was clearly visible. Just the inner brightening adjoining the dimming appears to be related to a stretched magnetic structure of the CME.

The conclusion of Yang and Chen (2010) that '...EIT wave propagates more slowly in the regions of stronger magnetic field' inspired us to compare near-surface EUV wave manifestations with the fast-mode speed ($V_{\rm fast}$) distribution.

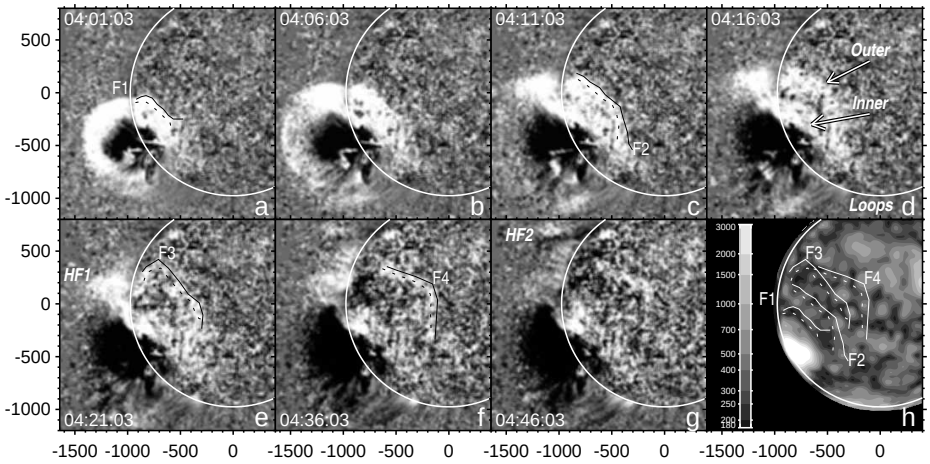


**Figure 4.** The EUV wave in fixed-base ratio EUVI 195 Å images (a – g) and $V_{\rm fast}$ distribution at 30 Mm (h). The white circles outline the solar limb. Some portions of the wave fronts are outlined with black contours F1 – F4 at their foremost (solid) and brightest (dotted) parts. The scale bar in panel h quantifies the $V_{\rm fast}$ levels in km s$^{-1}$.

Unlike the authors, we calculate $V_{\rm fast}$ from the *magnitude* of the magnetic field that determines the Alfvén velocity ($V_{\rm A}$) rather than any magnetic component. The magnetic field was extrapolated to 30 Mm from a SOLIS magnetogram observed at 19:30 on 20 January using potential approximation (Rudenko, 2001). A simplest way to obtain a $V_{\rm fast}$ distribution is to assume a constant temperature and to take densities, *e.g.*, from the Saito model. We attempted to get a somewhat more realistic density distribution using a SOHO/EIT 195 Å image observed on 20 January and an expression $\log n_e = 8.34 + 0.509 \log I_{195}$ obtained by Brosius *et al.* (2002) in a study of a particular region ($n_e$ is the electron density, $I_{195}$ is the brightness in the 195 Å EIT channel). This expression cannot be used everywhere, because the EUV brightness, $I_{195} \propto n_e^2 L$, depends on the depth $L$. However, $V_{\rm A}$ depends on the depth weakly, $\propto L^{1/4}$, and we restricted the density above quiet regions by limiting plasma beta $\beta \leq 0.65$. The sound speed was taken 180 km s$^{-1}$ everywhere. The resulting $V_{\rm fast}$ distribution is presented in Figure 4h. Most likely, the high-speed area in the active region was smaller on 17 January than the three-days later magnetogram shows (this does not affect our analysis). Also, the density could be underestimated there.

We have outlined four pronounced portions of the EUV wave fronts F1 – F4 both in EUVI images (a, c, e, and f) and on the $V_{\rm fast}$ distribution (h). The solid lines correspond to foremost visible fronts, and the dotted lines outline their brightest parts. Comparison with panel h shows that the EUV wave was brightest in regions of lowest $V_{\rm fast}$. The boundary of the EUV wave corresponded to regions, where $V_{\rm fast}$ increased. That is, the small-scale distribution of $V_{\rm fast}$ did not determine kinematics of the wave, but affected the brightness and sharpness of the wave front. Indeed, the Mach number $M = V_{\rm shock}/V_{\rm fast}$ increases in regions of reduced $V_{\rm fast}$, $\Delta M \approx -(M-1)\Delta V_{\rm fast}/V_{\rm fast}$, *i.e.*, the effect of the shock is stronger. In turn, kinematics of the shock wave was governed by the large-scale

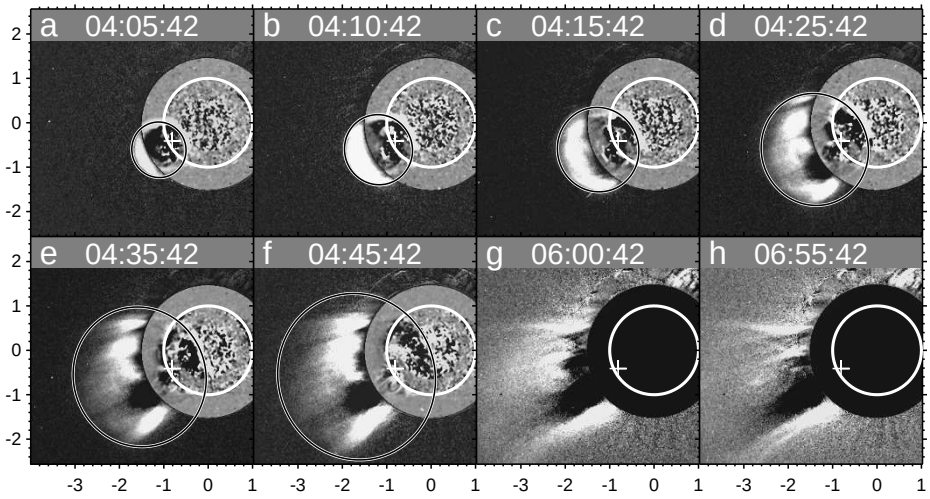


**Figure 5.** A white-light coronal transient in STEREO-B/COR-1 fixed-base difference images and the EUV wave fronts in corresponding running-difference EUVI images (a – f) from Figure 2 replacing the occulting disk. The thick white circle denotes the solar limb. The black-on-white oval outlines the outermost edge of the CME according to the shock-PL fit. The cross denotes the eruption site. The axes show distances from the solar disk center in solar radii.

$V_{\rm fast}$ distribution: the wave ran faster in the large-scale region around the polar coronal hole. These results address the issue raised by Yang and Chen (2010): no correlation is expected between the small-scale near-surface distribution of $V_{\rm fast}$ and the velocity of the whole shock front, when the wave has expanded enough.

### 2.4. White-light Coronal Transient Observed with COR-1 and LASCO/C3

Figure 5 presents eight selected images of a coronal transient observed with STEREO-B/COR-1. A fixed image observed at 03:50 was subtracted from all others. The outermost edge of the transient is outlined with ovals corresponding to the shock-PL fit with the same $t_0$. To keep the transient within the ovals, we progressively shifted their centers upwards-left in the plane of the sky according to the non-radial expansion of the wave dome (see Section 2.2) and used different expansion factors in the horizontal direction ($\delta_{\rm hor} = 2.80$) and the vertical one ($\delta_{\rm ver} = 2.85$). Thus, the front tended to become oblate. The positions of the ovals on the solar disk are close to the global fronts in Figure 2 at matching times.

The ovals cling to the outermost edges of the transient. The foremost parts look like a plasma flow, whose structure is determined by coronal rays. The leading edge decelerated, as follows from the shock-PL fit ($\delta < 3$), and kinematics corresponded to a freely propagating shock wave. A structure probably detectable in two later images in panels g and h might be the CME core.

Figure 6 presents four of 12 LASCO/C3 images, in which the CME is detectable at larger distances. Probable frontal structure and core are indicated in panel c. A presumable plasma flow seems to be present ahead. The fastest

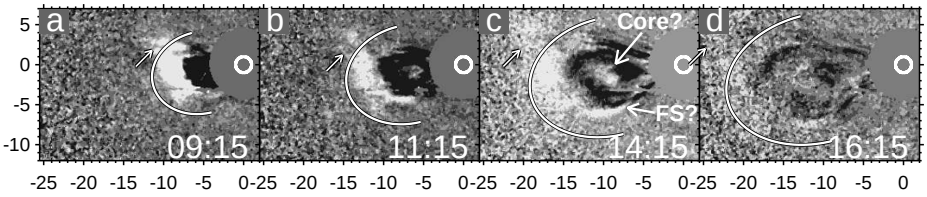


**Figure 6.** The CME observed with LASCO/C3. The thick white circle denotes the solar limb. The white-on-black oval outlines the outermost edge of the CME according to the shock-PL approximation. The arrow points at a fast accelerating feature measured in the SOHO LASCO CME Catalog at 06:15 – 16:15. The axes show distances from the solar disk center in solar radii.

feature measured at a position angle of 83° in the SOHO LASCO CME Catalog[2] accelerated. This feature, most likely of a non-wave nature due to its kinematics, is indicated by the arrow. We tried to outline the remainder part of the CME with an oval corresponding to expansion of the shock wave. The ovals in Figure 6 calculated according to the shock-PL fit with the same wave start time $t_0$, $\delta_{\rm hor} = 2.63$, $\delta_{\rm ver} = 2.43$, embrace all CME components but the fastest feature at 83°. Rather poor observations and the low CME speed ($< 400$ km s$^{-1}$) do not allow us to find out if the change of its shape could be due to effects of shock propagation or acceleration of the solar wind. Nevertheless, shock-wave kinematics does not contradict even LASCO/C3 observations up to $23R_\odot$.

### 2.5. Expansion of the EUV Wave Dome and the Type II Burst Drift Rate

A dynamic spectrum combined from HiRAS and Learmonth records is shown in Figure 7a. The type II burst had a single band most likely corresponding to the second harmonic, because the fundamental emission should be strongly refracted due to the location of the eruption site far behind the limb. Veronig *et al.* (2010) came to the same conclusion. The drift of the burst is well outlined with the PL model $n = 5.5 \times 10^8 (h/100\ {\rm Mm})^{-2.8}$ and the same wave start time $t_0$. The dashed outline corresponds to a presumable fundamental emission.

Figure 7b shows height-time measurements of the wave dome from EUVI 171 Å and 195 Å images along with a shock-PL fit of the 171 Å data and the frequency drift converted into the height-time plot. All the curves are close to each other. Figure 7c shows speed-time plots calculated from the 171 Å fit and from the fit of the type II burst drift. These values might be interesting to compare with routine estimates from drift rates of type II bursts. Figure 7d presents our PL density model along with the well-known models of Newkirk (1961) and Saito (1970). The Saito model was taken at $\phi = 18°$ corresponding to the position angle of the wave outline in COR-1 images. The PL model is close to the 2-fold Newkirk model at the onset of the type II burst, and then approaches the Saito model. The significant difference with the Newkirk model here, unlike the events considered in Paper I, might be due to the pronouncedly non-radial expansion of the wave.

[2]Yashiro *et al.* (2004); http://cdaw.gsfc.nasa.gov/CME_list/

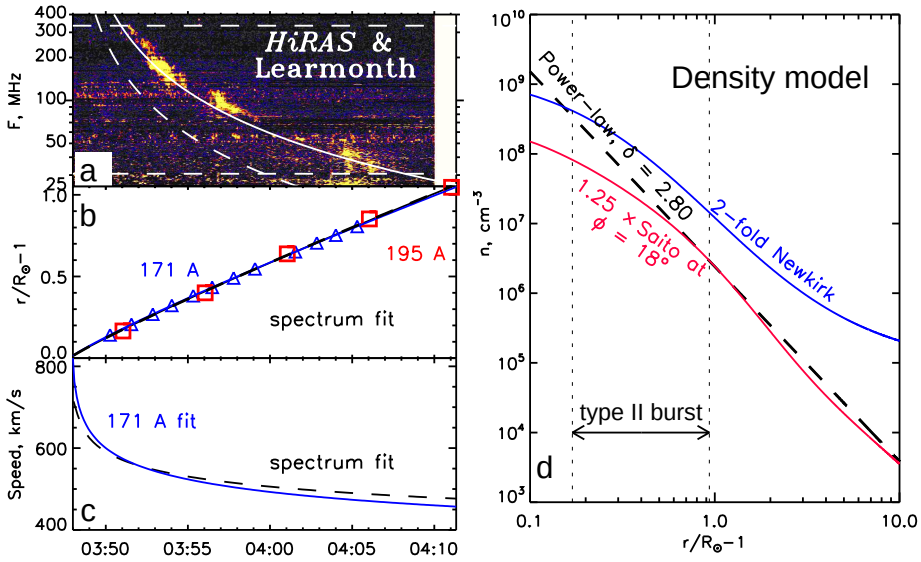


**Figure 7.** Expansion of the EUV wave and the type II burst. a) A dynamic spectrum composed from the HiRAS and Learmonth records. b) The height-time measurements from EUVI 195 Å images (red squares) and 171 Å ones (blue triangles) along with a shock-PL fit (blue line) and fit of the dynamic spectrum converted into heights (dashed black). c) The speed-time plots calculated from the shock-PL fit of the 171 Å data (blue) and from the dynamic spectrum (dashed black). d) Coronal density models: a PL model with $\delta = 2.8$ (dashed black) fitting the dynamic spectrum in panel (a) along with the models of Newkirk (blue) and Saito for $\phi = 18°$ (red). The vertical dotted lines delimit the interval corresponding to the type II burst.

## 3. Discussion

The detailed STEREO/SECCHI observations of the EUV wave both on the solar disk and above the limb allow us to compare the measurements performed in terms of the shock-PL fit proposed in Paper I with results of modeling in terms of the approach described in Paper II (WS model). The EUV wave propagated mainly over quiet Sun's regions without noticeable large-scale features except for the polar coronal hole. Since the EUV wave most likely was a near-surface trail of a large-scale coronal MHD wave, its kinematics should not be significantly affected by small-scale inhomogeneities, as the observations show indeed (Section 2.3). We describe global propagation of the EUV wave outside of the active region assuming only radial variations of coronal plasma parameters. The on-disk EUV wave decelerated from $\gtrsim 390$ to $\lesssim 290$ km s$^{-1}$ as our estimates in Section 2.1 suggest; Veronig *et al.* (2010) found broadening of the wave profile. These facts along with estimates of $V_{\rm fast}$ in the lower corona above the quiet Sun indicate that the shock wave was weak to moderate, and its deceleration was accompanied by broadening its profile (see Paper II). Thus, our WS model appears to apply.

The model is not yet able to incorporate coronal magnetic fields extrapolated from real magnetograms. We therefore model kinematics of only an on-disk wave running over the quiet Sun. We use the barometric density falloff of isothermal coronal plasma $n(r) = 4 \times 10^8 \exp\{9.71\,(R_\odot/r - 1)\}$ cm$^{-3}$ with coronal temperature $T = 1.5$ MK (sound speed 180 km s$^{-1}$), and the radial magnetic field model

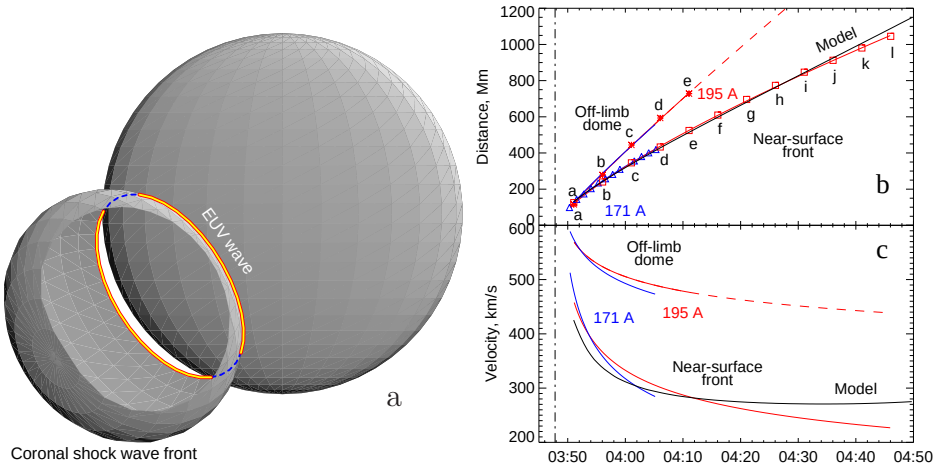


**Figure 8.** Measurements, fit, and modeling of shock front propagation. a) The modeled shock front. b) Distance-time plots of the on-disk wave (measured along the great circle in Figure 2) and the off-limb dome, their shock-PL fit, and a modeled plot. Red is related to 195 Å, blue is related to 171 Å, and black shows the model. c) The same for the calculated velocities.

$B_r = 1.35\,(R_\odot/r)^2$ G. $V_\mathrm{A} = 170$ km s$^{-1}$ at 40 Mm and increases upwards. We assume that the wave originates at an initial surface as large as 200 Mm, inside which the wave source is located. Then an EUV wave front can be observed at 03:51. The model shock wave has an initial length of 80 Mm and an amplitude of $1.5\,V_{\mathrm{fast}\,0}$ ($V_{\mathrm{fast}\,0}$ corresponds to the source height of 80 Mm). We search for EUV signatures of the coronal wave at a height of 40 Mm.

Figure 8 shows some results of the modeling and our measurements. Figure 8a presents the computed 3D shock front. The color rim is the section of the wave dome at 40 Mm. The on-disk EUV front could be partly covered by the dome. Figure 8b shows the distance-time plots of the on-disk EUV front measured from the 195 Å images (red squares) and 171 Å images (blue triangles). The red and blue lines show the corresponding shock-PL fit, and the black line presents results of the modeling. Figure 8c shows the velocity-time plots of the wave obtained by differentiating of the shock-PL curves and the modeled plot. The EUV wave appreciably decelerates due to damping and then slightly accelerates because of an increasing tilt of the front to the solar surface that is discussed in Paper II.

We have also modeled propagation of a shock wave upwards. Active regions determine a $V_\mathrm{A}$ distribution in their vicinities. To simulate this effect, we have added a magnetic dipole into our radial magnetic field model as Warmuth and Mann (2005) did. A 'horizontal' dipole seems to correspond to the active region on 17 January. Embedding such a dipole into the model results in strongly anisotropic $V_\mathrm{fast}$ distribution in the corona, with a domain of very low $V_\mathrm{fast}$ (about the sound speed near a null point of the magnetic field) and that of enhanced $V_\mathrm{fast}$. This causes asymmetric wave front propagation that was actually observed in our event. However, the domain of influence of a 'horizontal' dipole turns out to be too large, comparable with the solar hemisphere, whereas an estimate from the extrapolated magnetic field shows the domain of influence to

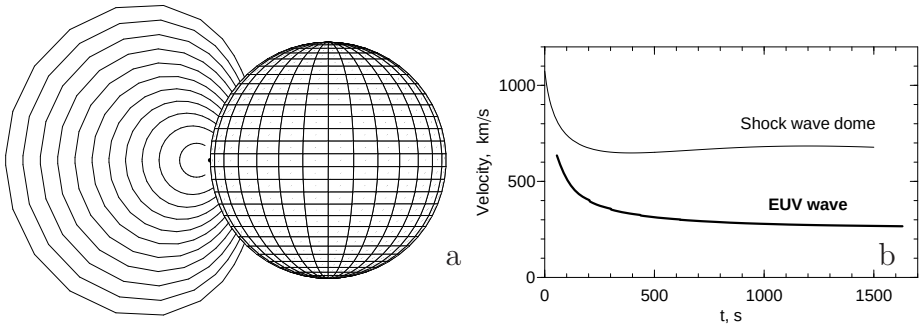


**Figure 9.** A freely propagating weak shock wave in the WS model containing an active region. a) Shock fronts separated by 2.5-min intervals. Note the progressive rise of the geometric wave center. b) Calculated shock front speeds upwards (thin) and along the solar surface (thick).

be rather compact along the solar surface ($\lesssim$ 260 Mm). Therefore, we employ the 'parallel' dipole, which provides a compact domain of enhanced $V_{\rm A}$. We adjust the height falloff of the magnetic field above the active region following Gary (2001), but decrease the magnetic field strength to obtain a realistic $V_{\rm fast}$ distribution with model parameters used.

Figure 9 shows model results. The wave source is located above the limb in the equatorial plane. The shock front is oblate in the radial direction presumably due to upwards increase of $V_{\rm fast}$ above quiet regions. The effect agrees with the COR-1 observations (Figure 5). The speed of the upwards wave expansion is about twice higher than that of the on-disk EUV wave (Figure 9b). This confirms our suggestion in Paper I to overcome the absence of correlation between the speeds of EUV waves and exciters of type II bursts stated by Klassen *et al.* (2000).

The twice-higher upwards speed of the EUV wave relative to the on-disk one prompted Veronig *et al.* (2010) that the upward dome expansion was driven all the time by the CME. The authors mentioned that the upward-lateral speed difference could be due to direction-dependent falloffs of $V_{\rm fast}$, but considered that the CME-driven option was favored by the limited lateral extent of the dimming. However, the latter fact only means that CME-related opening magnetic fields occurred in a limited region and did not propagate over large distances as Delannée and Aulanier (1999), Chen, Fang, and Shibata (2005), and Attrill *et al.* (2007) proposed. The major expansion of all CMEs is radial, but this fact does not guarantees that all CME-associated shocks are driven all the time.

The speed difference in Figure 9 was obtained for a *freely propagating wave* and the direction-dependent $V_{\rm fast}$ above the active region. The front shapes match the observations. The results agree with our considerations and measurements in Paper I and support the scenario of an impulsively generated freely propagating weak shock wave (see also Pomoell, Vainio, and Kissmann, 2008).

The WS modeling explains the disaccord between the EUV wave fronts identified by us and Veronig *et al.* (2010). Our red global EUV fronts in Figure 2 lag behind the blue fronts identified by the authors. The difference was most likely due to a projection effect combined with a different sensitivity of measurements as Figure 10 explains. Plasma is compressed by the shock front over the whole

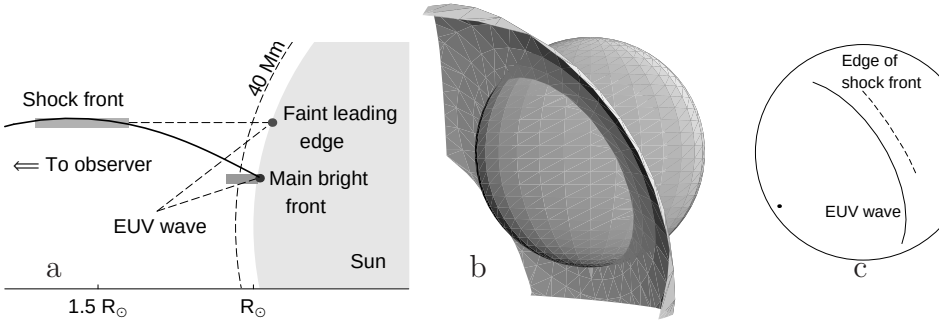


**Figure 10.** Modeling the situation at about 04:30. a) The relation between the foremost edge of the EUV wave and its main part. Thick horizontal bar shows cross section of the wave front presumably contributing to the foremost edge of the wave detected by Veronig *et al.* (2010). b) A portion of the modeled shock front. c) The lower edge (solid) of the shock front shown in panel (b) and a projection of the faint front's foremost edge (broken) on the solar surface.

its surface. The largest column emission measure of the compression region was near the solar surface, where the plasma density was higher. Veronig *et al.* (2010) probably detected a high outermost edge of the convex wave front. Figure 10a demonstrates the calculated 2D cross section of the wave front with its outermost edge at a height of $\approx 0.5R_\odot$. Figure 10b presents a portion of the modeled wave front. Figure 10c shows the calculated on-disk projections of the faint leading edge and the main bright EUV wave front corresponding to about 04:30. The situation resembles the seemingly disaccord between the measurements of Warmuth *et al.* (2004) and White and Thompson (2005) discussed in Section 'Event 4' of Paper I for a similar reason. We have reconciled the discrepancy in terms of the shock-PL approach by means of density falloff anisotropy: high density along the surface is nearly constant (low $\delta$) and deceleration is strong; the density falloff towards large altitudes is steeper (with $\delta = 3$ no deceleration occurs). In terms of the WS approximation, near the surface the $V_{\rm fast}$ is lower and damping is stronger that presumably results in stronger wave deceleration.

## 4. Summary and Concluding Remarks

Our analysis has confirmed the major conclusion of Veronig *et al.* (2010) that both the on-disk EUV wave and the dome expanding above the limb were due to a coronal shock wave. In addition to the authors' arguments, we have established that 1) the front shape and its changes, 2) kinematics of both the on-disk front and the off-limb dome up to $23R_\odot$, and even 3) the difference between our and the authors' measurements all corresponded to expected propagation of a shock wave. We have also found that, in agreement with the shock-wave hypothesis, kinematics of the global wave front 4) corresponded to the drift rate of the type II burst and 5) was controlled by large-scale distribution of the fast-mode speed, while its local inhomogeneities affected the brightness and sharpness of the EUV wave, *e.g.*, it was brightest in loci of the fast-mode speed minima.

We do not confirm the presumption of Veronig *et al.* (2010) that the shock wave was driven by the CME all the time. We do not see any support for this conjecture. On the contrary, we consider the shock wave to be excited by an impulsively erupting magnetic rope structure and freely propagating afterwards like a decelerating blast wave. This scenario was argued and observationally confirmed in Paper I. All the conclusions listed in the preceding paragraph are based on considerations and modeling of freely propagating shock waves.

The shock in this event was most likely weak, at least, near the solar surface. Model calculations for a weak shock match observations. Nevertheless, the self-similar shock approximation provides reasonable results up to distances $> 20R_{\odot}$ and even close to the early shock appearance, although with somewhat variable parameters, that confirms usefulness of this simple instrument.

We have revealed another large-scale EUV brightening presumably associated with a stretching CME structure. This 'inner' brightening was quasi-stationary. No manifestations of opening magnetic fields were found outside of the eruption region, while the 'outer' on-disk EUV wave was well visible there.

We specify the conclusion of Veronig *et al.* (2010) that the observed dome was not the CME. Indeed, the leading part most likely was not a magnetoplasma CME component. Coronagraph images, their shock-PL fit, and our considerations indicate that this was a plasma flow successively involved into the motion by the freely propagating shock front. The plasma flow was slower than the shock front (depending on the Mach number), whose speed was the phase velocity of this involvement. Thus, the leading part of the transient was a plasma flow, *i.e.*, a *coronal mass ejection* by definition, but it was a *shock-driven plasma flow*. This does not meet expectations of popular present concepts but has been anticipated (*e.g.*, R. Schwenn, 2004, private communication).

**Acknowledgements** We thank M. Temmer and A. Warmuth for fruitful discussions and S. Kalashnikov for the assistance in processing of the spectrograph data. We thank the teams operating all instruments whose data are used in our study for their efforts and open data policies: the ESA & NASA SOHO/EIT & LASCO and STEREO/SECCHI telescopes; the NICT HIRAS (Japan), the IPS Radio and Space Services Learmonth Observatory (Australia), and the USAF RSTN radio telescopes. We appreciatively use the CME catalog generated and maintained at the CDAW Data Center by NASA and the Catholic University of America in cooperation with the Naval Research Laboratory. SOLIS data used here are produced cooperatively by NSF/NSO and NASA/LWS. The research was supported by the Russian Foundation of Basic Research under grants 09-02-00115, 11–02–00038, and 11–02–00050.

## References

Afanasyev, An. N., Uralov, A. M.: 2011, *Solar Phys.* Submitted.
Attrill, G. D. R.: 2010, *Astrophys. J.* **718**, 494.
Attrill, G. D. R., Harra, L. K., van Driel-Gesztelyi, L., Démoulin, P.: 2007, *Astrophys. J.* **656**, L101.
Brosius, J. W., Landi, E., Cook, J. W., Newmark, J. S., Gopalswamy, N., Lara, A.: 2002, *Astrophys. J.* **574**, 453.
Brueckner, G. E, Howard, R. A., Koomen, M. J., Korendyke, C. M., Michels, D. J., Moses, J. D., *et al.*: 1995, *Solar Phys.* **162**, 357.
Chen, P. F., Fang, C., Shibata, K.: 2005, *Astrophys. J.* **622**, 1202.
Chen, P. F., Wu, S. T., Shibata, K., Fang, C.: 2002, *Astrophys. J.* **572**, L99.

Cohen, O., Attrill, G. D. R., Manchester, W. B., IV., Wills-Davey, M. J.: 2009, *Astrophys. J.* **705**, 587
Delaboudinière, J.-P., Artzner, G. E., Brunaud, J. *et al.*: 1995, *Solar Phys.* **162**, 291.
Delannée, C., Aulanier, G.: 1999, *Solar Phys.* **190**, 107.
Gallagher, P. T., Long, D. M.: 2010, *ArXiv e-prints*, arXiv:1006.0140.
Gary, G. A.: 2001, *Solar Phys.* **203**, 71.
Gopalswamy, N., Yashiro, S., Temmer, M., Davila, J., Thompson, W. T., Jones, S., McAteer, R. T. J., Wuelser, J.-P., Freeland, S., Howard, R. A.: 2009, *Astrophys. J.* **691**, L123.
Grechnev, V. V., Uralov, A. M., Slemzin, V. A., Chertok, I. M., Kuzmenko, I. V., Shibasaki, K.: 2008, *Solar Phys.* **253**, 263.
Grechnev, V. V., Uralov, A. M., Chertok, I. M., Kuzmenko, I. V., Afanasyev, An. N., Meshalkina, N. S., Kalashnikov, S. S., Kubo, Y.: 2011, *Solar Phys.* Submitted.
Howard, R. A., Moses, J. D., Vourlidas, A., Newmark, J. S., Socker, D. G., Plunkett, S. P., Korendyke, C. M., Cook, J. W. *et al.*: 2008, *Space Sci. Rev.* **136**, 67.
Kaiser, M. L., Kucera, T. A., Davila, J. M., St. Cyr, O. C., Guhathakurta, M., Christian, E.: 2008, *Space Sci. Rev.* **136**, 5.
Khan, J. I., Aurass, H.: 2002, *Astron. Astrophys.* **383**, 1018.
Kienreich, I. W., Temmer, M., Veronig, A. M.: 2009, *Astrophys. J.* **703**, L118.
Klassen, A., Aurass, H., Mann, G., Thompson, B. J.: 2000, *Astron. Astrophys. Suppl.* **141**, 357.
Liu, W., Nitta, N. V., Schrijver, C. J., Title, A. M., Tarbell, T. D.: 2010, *Astrophys. J.* **723**, L53.
Long, D. M., Gallagher, P. T., McAteer, R. T. J.. Bloomfield, D. S.: 2008, *Astrophys. J.* **680**, L81.
Newkirk, G. Jr.: 1961, *Astrophys. J.* **133**, 983.
Patsourakos, S., Vourlidas, A.: 2009, *Astrophys. J.* **700**, L182.
Patsourakos, S., Vourlidas, A., Wang, Y. M., Stenborg, G., Thernisien, A.: 2009, *Solar Phys.* **259**, 49.
Pomoell, J., Vainio, R., Kissmann, R.: 2008, *Solar Phys.* **253**, 249.
Rudenko, G. V.: 2001, *Solar Phys.* **198**, 5.
Saito, K.: 1970, *Ann. Tokyo Astr. Obs.* **12**, 53.
Thompson, B. J., Gurman, J. B., Neupert, W. M., Newmark, J. S., Delaboudinière, J.-P., St. Cyr, O. C., Stezelberger, S., Dere, K. P. *et al.*: 1999, *Astrophys. J.* **517**, L151.
Thompson, B. J., Plunkett, S. P., Gurman, J. B., Newmark, J. S., St. Cyr, O. C., Michels, D. J.: 1998, *Geophys. Res. Lett.* **25**, 2465.
Veronig, A. M., Muhr, N., Kienreich, I. W., Temmer, M., Vršnak, B.: 2010, *Astrophys. J.* **716**, L57.
Veronig, A. M., Temmer, M., Vršnak, B.: 2008, *Astrophys. J.* **681**, L113.
Warmuth, A., Mann, G.: 2005, *Astron. Astrophys.* 435, 1123.
Warmuth, A., Vršnak, B., Aurass, H., Hanslmeier, A.: 2001, *Astrophys. J.* **560**, L105.
Warmuth, A., Vršnak, B., Magdalenić, J., Hanslmeier, A., Otruba, W.: 2004, *Astron. Astrophys.* **418**, 1101.
Wills-Davey, M. J., Attrill, G. D. R.: 2009, *Space Sci. Rev.* **149**, 325.
White, S. M., Thompson, B. J.: 2005, *Astrophys. J.* **620**, L63.
Yang, H. Q., Chen, P. F. 2010, *Solar Phys.* **266**, 59.
Yashiro, S., Gopalswamy, N., Michalek, G., St. Cyr, O. C., Plunkett, S. P., Rich, N. B., Howard, R. A.: 2004, *J. Geophys. Res.* 109, A07105.
Zhukov, A. N., Auchère, F.: 2004, *Astron. Astrophys.* **427**, 705.
Zhukov, A. N., Rodriguez, L., de Patoul, J.: 2009, *Solar Phys.* **259**, 73.